Improving the Flight Path Marker Symbol on Rotorcraft Synthetic Vision Displays

Zoltan P. Szoboszlay
Army/NASA Rotorcraft Division, Aeroflightdynamics Directorate
US Army Aviation and Missile Research, Development, and Engineering Center
Ames Research Center, Moffett Field, CA 94035-1000

Gordon H. Hardy
Northrop Grumman Information Technology
Moffett Field, CA 94035

Terence M. Welsh
Silicon Valley Systems
Sunnyvale, CA 94087

Two potential improvements to the flight path marker symbol were evaluated on a panel-mounted, synthetic vision, primary flight display in a rotorcraft simulation. One concept took advantage of the fact that synthetic vision systems have terrain height information available ahead of the aircraft. For this first concept, predicted altitude and ground track information was added to the flight path marker. In the second concept, multiple copies of the flight path marker were displayed at 3, 4, and 5 second prediction times as compared to a single prediction time of 3 seconds. Objective and subjective data were collected for eight rotorcraft pilots. The first concept produced significant improvements in pilot altitude control, ground track control, workload ratings, and preference ratings. The second concept did not produce significant differences in the objective or subjective measures.

Introduction

Army rotorcraft pilots routinely fly at low altitudes, using the terrain to mask the aircraft against radar and visual detection. Decades ago, low-altitude operations were restricted to daylight, clear weather, visual conditions. The development of night vision devices enabled a substantial increase in the percentage of time available for low altitude helicopter operations, in addition to enabling the use of the night environment to mask the aircraft against visual detection. However, there remains one visual condition in which most Army rotorcraft cannot operate low level: degraded visual environments due to weather, dust, or smoke. Poor visibility conditions can restrict both daylight and night operations for days at a time. Synthetic vision display systems offer a potential tool for enabling pilots to fly in poor visibility conditions. In synthetic vision systems, an image of the terrain is rendered from either a stored terrain database, or a sensor. (The term "enhanced vision" is often used for sensor-derived images; that distinction is not made in this paper.)

There are many similarities between a synthetic vision display and a night vision display. In both cases, a perspective-view image of the terrain appears on the display. In both cases, the Field-of-View (FOV) of the terrain image is a small fraction of the pilot's clear weather, daylight, out the window view. In both cases, reduced resolution and contrast diminish the usable ground texture as compared to the pilot's clear weather, daylight, out-the-window view. Night vision systems have not enabled the rotorcraft pilot to operate at night with the same level of safety as daylight operations (Refs. 1, 2). Similarly, pilots flying synthetic vision systems will probably not have the same level of safety as they have in clear-visibility, daylight operations. The importance of completing the mission in a timely manner, and the hazard of operating in hostile territory during clear-weather conditions must be weighed against the extra hazards of operating in poor visibility using synthetic vision systems. Synthetic vision systems may also add a measure of safety for the cases of inadvertent flight into poor and marginal visibility conditions.

To compensate for the deficiencies of using a display for pilot awareness of self-motion through the terrain, aircraft state information is added in the form of computer graphics and text. Typical state information includes attitude, altitude, and speed. Because of the similarities between synthetic vision displays and night vision displays, the symbology (graphics and text) is expected to be nearly identical between the night vision system and synthetic vision system with one major exception. Synthetic vision systems have knowledge of the terrain elevations ahead of the aircraft, whereas typical night vision systems do not have this information available. The synthetic vision display detailed in this paper takes advantage of the knowledge of terrain elevations ahead of the aircraft to improve flight symbology. In addition, a concept of showing the predicted position of the aircraft at multiple prediction times was also evaluated.

Presented at the American Helicopter Society 60th Annual Forum, Baltimore, MD, June 7-10, 2004.

Relation to Previous Work

The Flight Path Marker (FPM) became a standard symbol on primary flight displays to indicate the vertical and lateral direction of travel (Fig. 1, Ref. 3). When placed on a display with an image of the terrain in the background, and with proper scaling, the FPM symbol shows the location the aircraft is moving toward with respect to the terrain. Recent examples of this symbol on rotorcraft displays are found on the AH-64D and the V-22 aircraft.

Fig. 1. MIL-STD-1787 Flight Path Marker (FPM).

An improvement to the FPM symbol was to "quicken" the movement so that the FPM showed either the predicted direction of travel, or the predicted position in space at a predetermined time in the future. A Quickened Flight Path Marker (QFPM) reacts much faster to the pilot's control inputs than a FPM driven only by the aircraft dynamics. The pilot therefore tends to have less overshoot of required control stick inputs with the QFPM as compared to the FPM.

In conjunction with the QFPM symbol, other symbols were added to provide guidance along a precise, 3D path to a landing. One symbol is the leader aircraft, and is shown in Fig. 2 as implemented on the Rotorcraft Aircrew Systems Concepts Airborne Laboratory (RASCAL) UH-60 helicopter (Ref. 4). The leader is shown in perspective view on the 3D predetermined path a fixed time in the future. The prediction time of the QFPM is set to the same time in the future as the leader. By manipulating the flight controls to place the QFPM symbol over the leader aircraft symbol, the pilot converges on the predetermined 3D path. The other common guidance symbol is the pathway-in-the-sky (or tunnel-in-the-sky) symbol, also shown in Fig. 2.

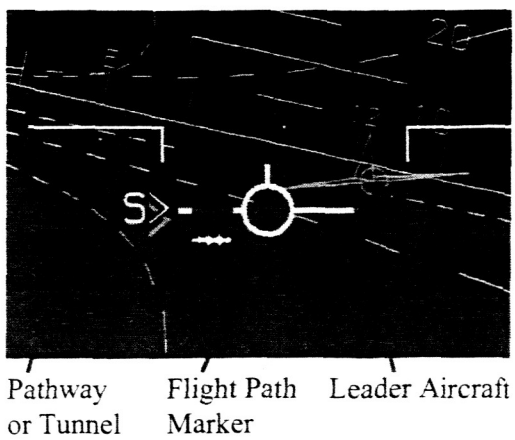

Fig. 2. Pursuit guidance display.

QFPMs and path guidance symbols for VTOL aircraft were flown in simulations (Refs. 5, 6), AV-8B flight test (Ref. 7), and XV-15 flight test (Ref. 8) for precision approaches to hover-pads and runways. This symbol was also flown in STOL simulation (Ref. 9) and flight (Ref. 10) for precision runway landings.

For the Automated Nap-Of-the-Earth (ANOE) program, both the QFPM concept, and the 3D guidance concept (leader and pathway) were applied to the task of flying low level, in poor visibility, with terrain following and terrain avoidance (Refs. 11, 12). In simulation, and flight on a UH-60, an ideal 3D pathway was produced continuously based on current position, long-term desired path, and nearby terrain as determined by an on-board terrain database. These tests demonstrated the utility of the pursuit guidance and pathway-in-the-sky symbols for rotorcraft terrain-following/terrain-avoidance tasks at an altitude of 200 ft. Above Ground Level (AGL).

At the end of the ANOE program, a new symbol was introduced in simulation called a Reference Point (RP), as shown in Fig. 3 (Ref. 13). The purpose of the symbol was to provide predicted height and predicted ground track information when the pilot intentionally flew off the computed path, or flew without a pre-programmed path. The RP symbol was drawn as a triangle. The bottom vertex of the RP triangle showed the predicted point on the terrain that the aircraft was expected to fly over, 8 seconds in the future. In the lateral direction, the task of the pilot was to place the vertex of the RP symbol on the desired ground track. The height of the RP triangle was set to the target altitude AGL. The vertical control task of the pilot was to put the QFPM symbol at the same height as the top edge of the RP triangle. The QFPM and RP symbols were not constrained to be in-line vertically.

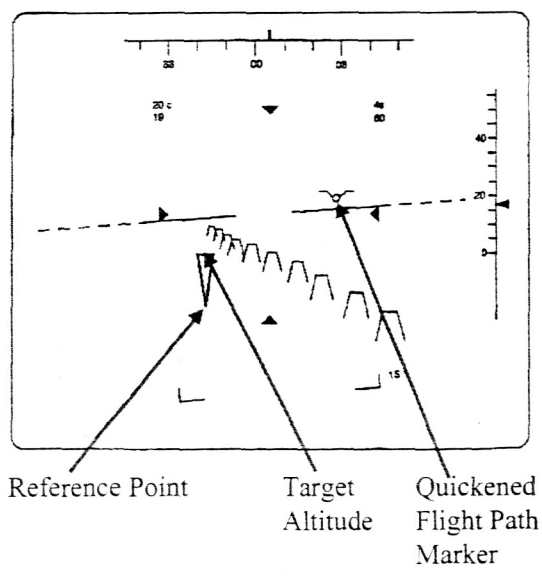

Fig. 3. Symbology used in Ref. 13. showing the RP and QFPM.

The simulation in Ref. 13 was flown in poor visibility conditions, at nominally 20 foot altitude AGL, and 15-25 knots speed. Although there were not enough pilots in the simulation to gather statistically significant results, there was a trend, when using the RP symbol, of improved altitude control, and improved workload scores. There was also an observation during the experiment of poor airspeed control.

Under the US Army Small Business Innovative Research (SBIR) program, two other symbology concepts were implemented by Anacapa Sciences Inc. in a helicopter simulation. These concepts were intended to aid the pilot during low-level flight, day and night (clear visibility), without a predetermined path (Ref. 14). One concept, shown in Fig. 4, was drawing multiple copies of the QFPM at prediction times of 1, 2, 3, 4, and 5 seconds in the future. The second concept tested was the display of two lines, drawn 25 feet on either side of the predicted ground track, also shown in Fig. 4. The multiple QFPMs and predicted ground track were always drawn together in one display condition. That display condition was then compared to the same symbology set without the QFPMs and predicted ground track. Eight pilots flew a slalom course at varying speeds and to altitudes up to 60 feet. The combination of multiple QFPMs and predicted ground track in the Anacapa study significantly improved performance in the measures of the number of ground strikes, and mean roll direction changes. Workload ratings were reduced by a mean of 40% when the QFPMs and predicted ground track were present.

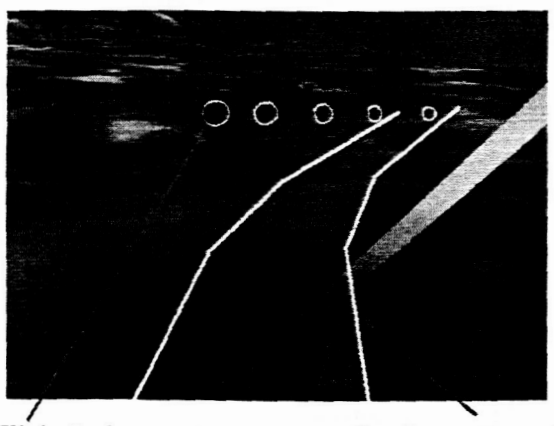

Fig. 4. Symbology developed by Anacapa Sciences Inc. (Ref. 14) showing multiple QFPMs and predicted ground track.

For the research detailed in this paper, the desired goal was to develop a display for flying a constant, low-AGL altitude, in poor visibility conditions including poor weather. One element of the design is to draw a "synthetic" image of the terrain from either radar data or a stored terrain database. The other portion of the design is drawing guidance symbols to aid the pilot in predicting the altitude and ground track given the current state of the aircraft and control inputs. If a predetermined 3D course is available, then the leader aircraft and/or pathway-in-the-sky concepts previously demonstrated should be adequate. However, if a predetermined 3D course is not available (as is the usual case), then guidance information similar to Refs. 13 and 14 should be used. This experiment examines a symbol that is similar to the RP symbol, but combines the QFPM and RP symbols into one symbol. This experiment also examines whether multiple copies of the combined QFPM/RP symbol improve performance or reduce workload.

Method

A cab was constructed that had a three-axis, side-arm, cyclic control stick and a conventional collective (Fig. 5). The helicopter model was the NASA-Ames developed Enhanced Stability Derivative model with a rate-command, attitude hold control type for pitch and roll (Ref. 15). In the yaw axis, the control system had automatic turn coordination so yaw inputs were unnecessary. Winds were not simulated. A 10-inch diagonal, liquid-crystal display was used for this experiment for the synthetic vision, primary flight display. A 50 degree (horizontal) field-of-view, color, photo-texture image of the terrain was drawn. The worst-case visibility condition was simulated; no out the window view was provided, and only a synthetic image of the terrain was available on the primary flight display.

Fig. 5. Synthetic vision simulation cab.

A basic MIL-STD-1295 symbol set was implemented across all display conditions as shown in Fig. 6 (Ref. 16). These symbols were not tested, but are necessary for basic control of the aircraft. This MIL-STD-1295 symbol set is essentially the same as implemented on the AH-64A aircraft with two changes. The first change was that the horizon line was uncompressed and earth referenced (unlike the AH-64A symbol which is compressed in the pitch axis and therefore non-conformal with the terrain image). The second change was that the radar altimeter digits incremented in 1-foot increments for the entire range.

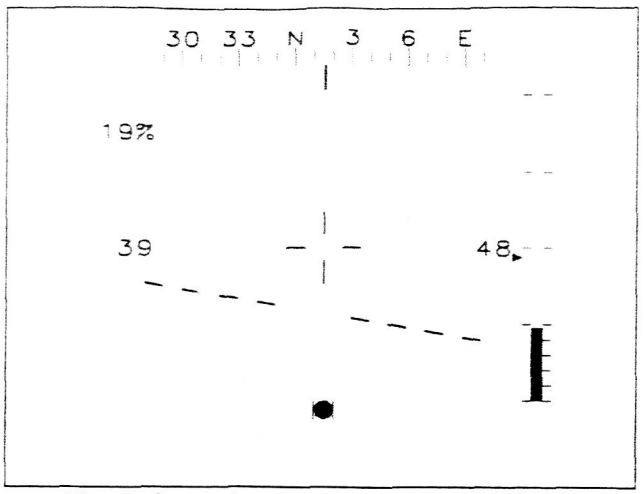

Fig. 6. Symbology common to all conditions.

This experiment tested variations of an altitude-predicting FPM shown in Fig. 7. The circle shows the predicted 3D position of the aircraft, 3 seconds in the future. This portion of the symbol is a QFPM discussed earlier, with the wing and tail icons removed to have less clutter. The intersection of the two convergent lines below the QFPM shows the location of the point on the terrain that the aircraft is expected to fly over in 3 seconds. That location is the projection of the QFPM onto the terrain. The diamond is the target altitude, drawn 50 feet above the projection point. To maintain a nearly constant altitude above the terrain, the pilot puts in enough collective stick input to place the QFPM (circle) over the target altitude symbol (diamond). In the lateral direction, the three parts of the altitude-predicting FPM symbol move together. The control strategy for the pilot is to put in enough lateral cyclic control stick input to place the projection point over the desired ground track seen on the terrain image.

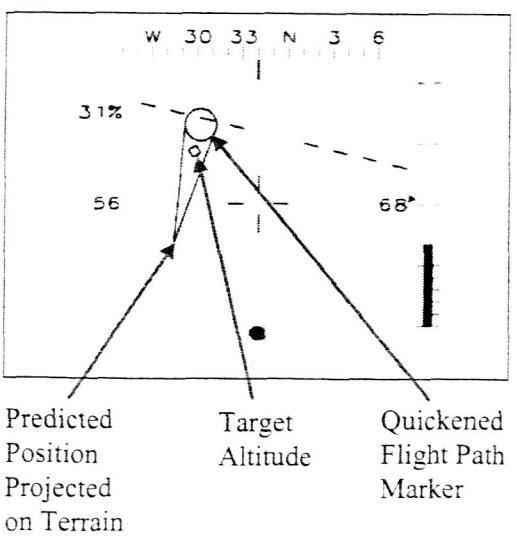

Fig. 7. Altitude Predicting Flight Path Marker.

The main conditions of the experiment were variations of the QFPM, set to form a 2x2 matrix as shown in Fig. 8. One factor was the presence or absence of predictive altitude information on the QFPM. The other factor was whether single or multiple QFPMs were presented to the pilot. The time of prediction for the single QFPM was set to 3 seconds. In the case of multiple QFPMs, the times were set to 3, 4, and 5 seconds. The drive equations for the predicted location of the aircraft (the circle) were identical for the four main conditions and are provided in appendix A. Pilots first flew the course at least three times for practice for each main condition. This practice session was then followed by a sequence of two more practice runs and a data run for each condition. The order of the four main conditions was counterbalanced using a Latin-square order.

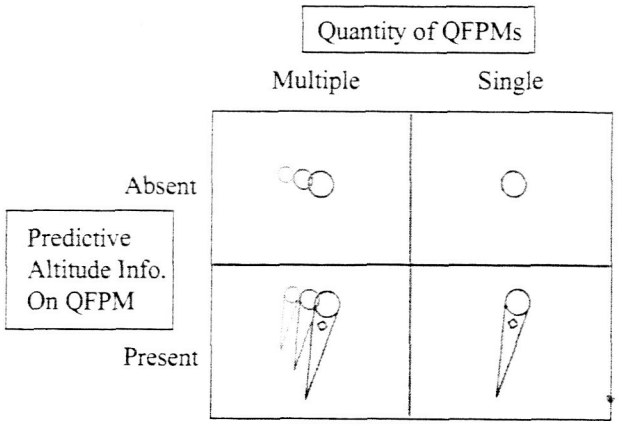

Fig. 8. Main experiment matrix.

Additionally, a baseline symbol set was flown by all pilots which had an Instantaneous Flight Path Marker (IFPM) as part of the symbol set (Fig. 9). This IFPM displays the current direction of motion of the aircraft with respect to the terrain image, and is the same as flown on the AH-64D and V-22. The IFPM symbol set was practiced five times and then flown for data collection only after data collection was completed for all the QFPMs.

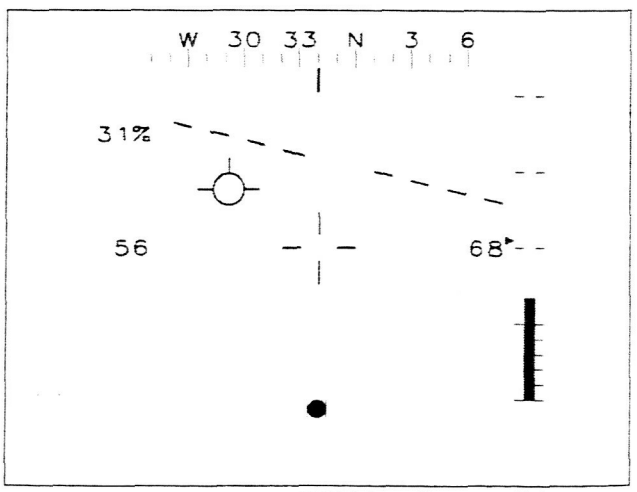

Fig. 9. Instantaneous FPM baseline condition.

During preliminary trials, experimenters and pilots noticed that when pitch inputs were put into the cyclic, a slow and steady airspeed change would occur over a long period of time. Often the pilot was not aware of the slowly increasing or decreasing airspeed until the airspeed was off by a factor of two. This problem was probably worse in the simulator, since the pilot was denied motion, sound, vibration, and out-the-window views. Since constant airspeed was desirable in this experiment in order to keep the course difficulty the same, pilots were trained to not put in cyclic pitch input, which kept airspeed constant throughout the maneuver. Only collective was used to control altitude; there was plenty of torque margin to complete the course with collective altitude control. Cyclic roll was used to control ground track.

Each pilot flew the same course for every display condition. The course was approximately 6 kilometers long, had sinusoidal turns of increasing sharpness, and had a number of hills as shown in Figs. 10 and 11. The pilots started at 50 knots airspeed and 50 foot altitude AGL. Pilots were tasked to maintain airspeed and altitude for the duration of the run, while flying a ground track over the marked course. Pilots were informed of all measures that were taken before data collection started.

Seven of the eight pilot participants were military-trained rotorcraft pilots with 3000+ hours rotorcraft experience. One pilot had 500+ hours of rotorcraft experience in addition to 10,000+ hours fixed wing experience. Five of the eight pilots were test pilots. Meeting FAA or military requirements for being current in an airframe was not required for this experiment.

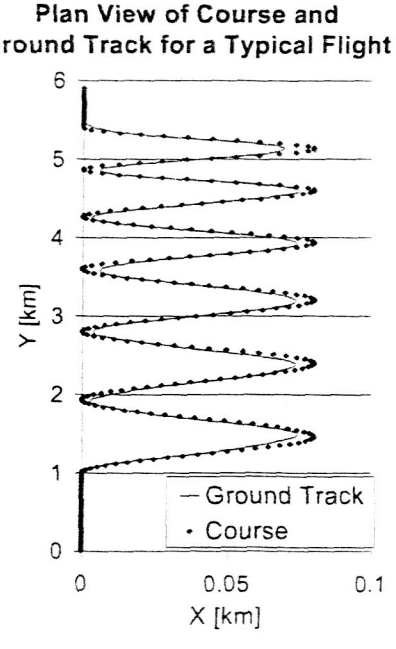

Fig. 10. Plan view of course and typical ground track (note the x-axis scale has been expanded.)

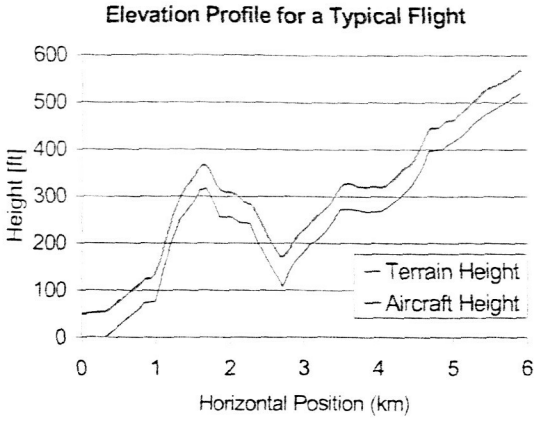

Fig. 11. Elevation of terrain and aircraft path for a typical flight (note height scale has been expanded.)

One measure of performance was altitude AGL. Root Mean Square (RMS), maximum high, and maximum low deviations from the 50 ft. target were analyzed. Another measure of performance was RMS and maximum horizontal deviations from the course.

As a measure of workload, NASA-TLX ratings were taken (Ref. 17). The ratings were weighted equally for all categories. A preference score was also taken as the final measure at the end of all data runs. Here, the pilots were asked to rate the most desired symbol set as a "1", through the least desired symbol set as a "5".

For the entire experiment, only one crash occurred during a data run. That single crash occurred for the condition of a single QFPM with no altitude information on the QFPM. The data from that run are not part of any data analysis in this report.

Results

Data are first analyzed as a 2x2 factorial design. Factor "A" is the presence or absence of predictive altitude information on the QFPM. Factor "B" is the number of QFPMs (single vs. multiple). Figs. 12 and 13 show the RMS and maximum horizontal deviation from the course, respectively. In both measures, there is a large improvement in performance when predictive altitude information is present on the QFPM as compared to absent (factor A). A criterial of $p<0.05$ is used in the Analysis of Variance (ANOVA). As the ANOVA shows in Table 1 and 2, the difference in mean performance for factor A is significant for the RMS error and significant for the maximum error. The difference in mean performance for single vs. multiple QFPMs (factor B) however, is not significant. The ANOVA result for an interaction between factor A and factor B is also not significant. As far as horizontal ground track deviation from the course, no advantage or disadvantage could be measured for multiple QFPMs as compared to a single QFPM (factor B).

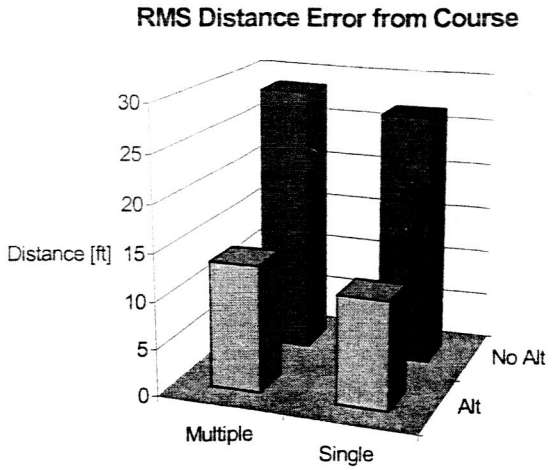

Fig. 12. RMS horizontal distance error from course.

Table 1. RMS horizontal distance error from course

2 x 2 ANOVA		
	Mean	**Std. Dev.**
Single-With Alt	11.40	2.40
Single-No Alt	26.75	6.82
Multiple-With Alt	13.42	3.54
Multiple-No Alt	28.49	8.16
	F Ratio	**p**
Factor A	F(1, 7) = 45.80	Signif, p < 0.01
Factor B	F(1, 7) = 2.63	Not significant
Interaction A x B	F(1, 7) = 0.04	Not significant
Factor A is presence or absence of alt. info. on QFPM. Factor B is single vs. multiple QFPMs.		

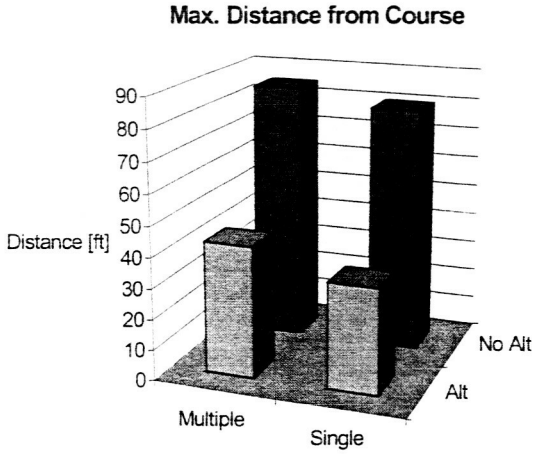

Fig. 13. Max. horizontal distance error from course.

Table 2. Max. horizontal distance error from course

2 x 2 ANOVA		
	Mean	**Std. Dev.**
Single-With Alt	34.41	7.69
Single-No Alt	80.05	19.56
Multiple-With Alt	42.90	13.57
Mult-No Alt	84.87	20.96
	F Ratio	**p**
Factor A	F(1, 7) = 38.81	Signif. p < 0.01
Factor B	F(1, 7) = 1.64	Not significant
Interaction A x B	F(1, 7) = 0.26	Not significant
Factor A is presence or absence of alt. info. on QFPM. Factor B is single vs. multiple QFPMs.		

In the case of multiple QFPMs, the drive equations used for determining the lateral displacement of the QFPMs differed in the time of prediction (3, 4, or 5 seconds). For the vertical displacement the QFPMs, the same drive equations were used, which gave the predicted steady state climb angle, and did not include a term for time. The steady state climb angle is desirable because the pilot can see immediately how much collective or cyclic-pitch input to make, without waiting for the slower aircraft response. However, this implementation of the drive equations caused the three QFPMs to move vertically the same amount in response to a collective or cyclic-pitch input. Rather than use a less desirable (and less standard) set of equations in the vertical direction that would provide a time dependent estimated position, the 2x2 ANOVA of performance data were restricted to the horizontal ground track. Altitude data are therefore not analyzed with a 2x2 ANOVA.

Figure 14 and Table 3 show the TLX ratings, which are used as a measure of workload. The TLX ratings are consistent with the horizontal ground track data: There was significant improvement in ratings (lower ratings) when predicative altitude information was added to the QFPM (factor A). There was no significant difference in TLX ratings for factor B or an interaction between factor A and factor B.

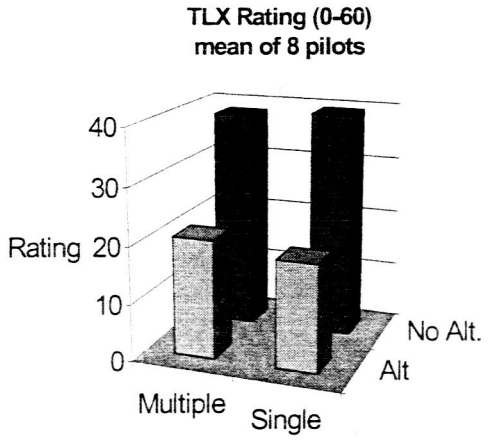

Fig. 14. TLX rating.

Table 3. TLX rating

2 x 2 ANOVA		
	Mean	**Std. Dev.**
Single-With Alt	18.73	5.95
Single-No Alt	39.49	6.52
Multiple-With Alt	20.80	5.19
Mult-No Alt	38.45	6.28
	F Ratio	**p**
Factor A	F(1, 7) = 36.40	Signif., p < 0.01
Factor B	F(1, 7) = 0.36	Not significant
Interaction A x B	F(1, 7) = 1.94	Not significant
Factor A is presence or absence of alt. info. on QFPM. Factor B is single vs. multiple QFPMs.		

Figure 15 and Table 4 show the preference ratings. Data show a very strong pilot preference (lower score) for having predictive altitude information on the QFPM. As with previous 2x2 results, there is a significant difference in means for factor A, no significant difference for factor B, and no significant interaction between factors A and B.

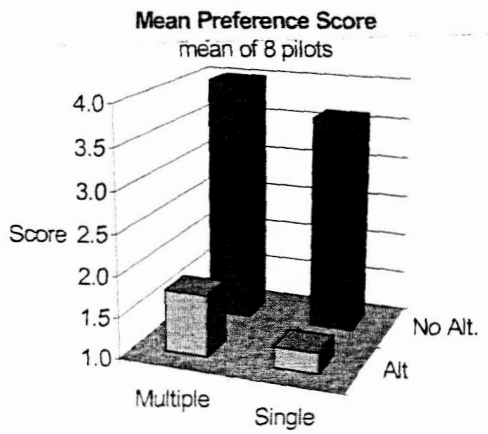

Fig. 15. Mean preference score.

Table 4. Mean preference score

2 x 2 ANOVA		
	Mean	**Std. Dev.**
Single-With Alt	1.25	0.46
Single-No Alt	3.63	0.52
Multiple-With Alt	1.75	0.46
Mult-No Alt	4.00	0.93
	F Ratio	**p**
Factor A	F(1, 7)=203.89	Signif., p < 0.01
Factor B	F(1, 7) = 1.60	Not significant
Interaction A x B	F(1, 7) = 0.18	Not significant
Factor A is presence or absence of alt. info. on QFPM. Factor B is single vs. multiple QFPMs.		

At this point, factor B (single vs. multiple QFPMs) is dropped from further analysis. The remaining analysis examines only the single FPMs. In particular, the cases examined are the single QFPM with predictive altitude information (condition #1), the single QFPM without predictive altitude information (condition #2), and the baseline IFPM, also without predictive altitude information (condition #3). Pair-wise comparisons are made on the three combinations of these conditions, and the Bonferroni criteria is applied to the ANOVA results to insure that performing multiple ANOVA tests, as opposed to a single test, does not aid in finding statistically significant results.

For all measures (Figs. 16-22 and Tables 5-11) the results are the same:

1) Significant improvement was recorded in the mean performance or rating for condition 1 compared to condition 2 or condition 3.

2) A reduction was recorded in the value of the standard deviation for condition 1 compared to condition 2 or condition 3 in the objective measures. In the subjective measures there are only small differences in the standard deviations. The standard deviation is a measure of the pilot-to-pilot variability in performance or rating.

3) No significant differences in the mean performance or ratings were seen between conditions 2 and 3. Both these conditions do not have predicted altitude information on the FPM. Condition 2 is quickened, and shows the predicted location in 3D space. Condition 3 is not quickened, and shows the instantaneous direction of travel.

Figure 16 shows a factor of four improvement in the mean performance for RMS altitude error from the 50 foot target altitude for condition 1 as compared to conditions 2 and 3.

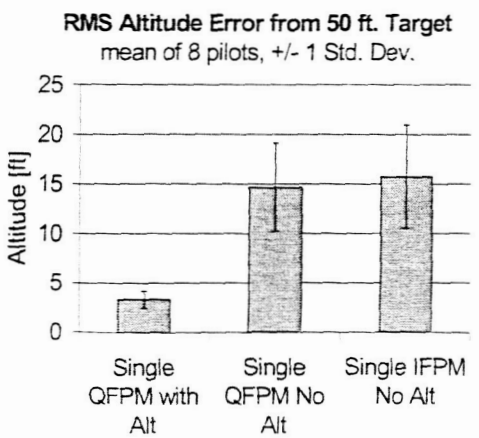

Fig. 16. RMS altitude error.

Table 5. RMS altitude error

(3) 1x2 ANOVA		
	Mean	**Std. Dev.**
#1	3.33	0.86
#2	14.63	4.44
#3	15.70	5.22
	F Ratio	**p**
1 vs. 2	F(1, 7) = 57.69	Signif., p < 0.01*
1 vs. 3	F(1, 7) = 47.70	Signif., p < 0.01*
2 vs. 3	F(1, 7) = 1.36	Not significant
Condition #1 is single QFPM with altitude information. Condition #2 is single QFPM without altitude info. Condition #3 is single IFPM without altitude info. * meets Bonferroni criteria		

Figure 17 shows an improvement by almost a factor of three in the mean performance for maximum altitude error above the 50 foot target altitude for condition 1 as compared to conditions 2 and 3. Reduction of altitude is important for an Army mission to prevent detection by radar.

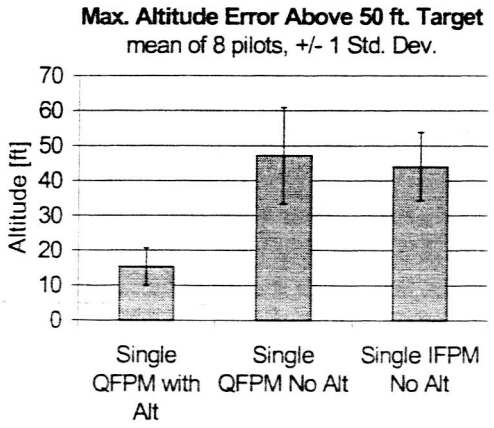

Fig. 17. Max. altitude error above the 50 ft. target.

Table 6. Max. altitude error above the 50 ft. target

(3) 1 x 2 ANOVA		
	Mean	**Std. Dev.**
#1	15.29	5.35
#2	47.12	13.81
#3	43.97	9.79
	F Ratio	**p**
1 vs. 2	F(1, 7) = 39.66	Signif., p < 0.01*
1 vs. 3	F(1, 7) = 38.67	Signif., p < 0.01*
2 vs. 3	F(1, 7) = 0.53	Not significant
Condition #1 is single QFPM with altitude information. Condition #2 is single QFPM without altitude info. Condition #3 is single IFPM without altitude info. * meets Bonferroni criteria		

Figure 18 shows a factor of two improvement in maximum altitude error below the 50 foot target altitude for condition 1 as compared to conditions 2 and 3.

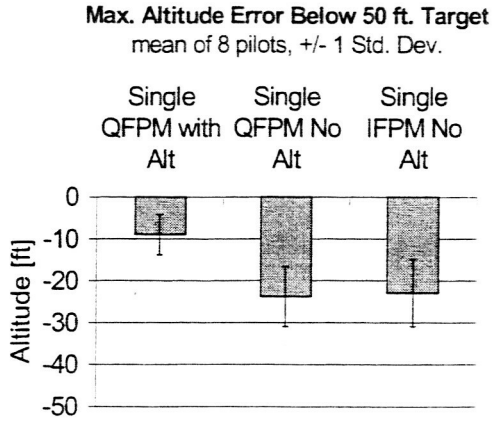

Fig. 18. Max. altitude error below the 50 ft. target.

Table 7. Max. altitude error below the 50 ft. target

(3) 1 x 2 ANOVA		
	Mean	**Std Dev.**
#1	-9.05	4.78
#2	-23.84	7.14
#3	-22.98	8.02
	F Ratio	**p**
1 vs. 2	F(1, 7) = 91.00	Signif., p < 0.01*
1 vs. 3	F(1, 7) = 41.50	Signif., p < 0.01*
2 vs. 3	F(1, 7) = 0.09	Not significant
Condition #1 is single QFPM with altitude information. Condition #2 is single QFPM without altitude info. Condition #3 is single IFPM without altitude info. * meets Bonferroni criteria		

Figure 19 shows a factor of two improvement in RMS horizontal deviation from the course for condition 1 as compared to conditions 2 and 3.

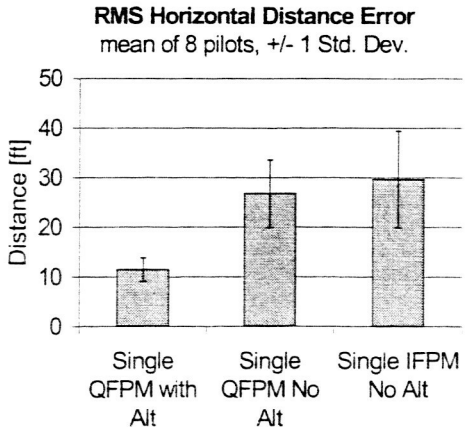

Fig. 19. RMS horizontal distance error.

Table 8. RMS horizontal distance error

(3) 1 x 2 ANOVA		
	Mean	**Std. Dev.**
#1	11.40	2.40
#2	26.75	6.82
#3	29.63	9.72
	F Ratio	**p**
1 vs. 2	F(1, 7) = 45.75	Signif., p < 0.01*
1 vs. 3	F(1, 7) = 30.47	Signif., p < 0.01*
2 vs. 3	F(1, 7) = 0.49	Not significant
Condition #1 is single QFPM with altitude information. Condition #2 is single QFPM without altitude info. Condition #3 is single IFPM without altitude info. * meets Bonferroni criteria		

Figure 20 shows a factor of two improvement for the maximum horizontal deviation from the course for condition 1 as compared to conditions 2 and 3.

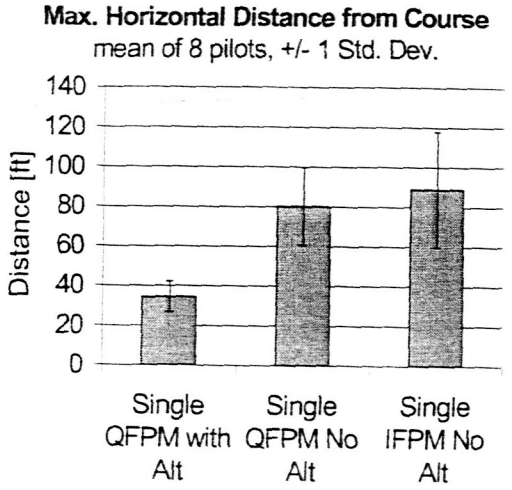

Fig. 20. Max. horizontal distance error from course.

Table 9. Max. horizontal distance error from course

(3) 1 x 2 ANOVA		
	Mean	**Std. Dev.**
#1	34.41	7.69
#2	80.05	19.56
#3	88.80	29.05
	F Ratio	**p**
1 vs. 2	F(1, 7) = 35.90	Signif., p < 0.01*
1 vs. 3	F(1, 7) = 22.19	Signif., p < 0.01*
2 vs. 3	F(1, 7) = 0.34	Not significant
Condition #1 is single QFPM with altitude information. Condition #2 is single QFPM without altitude info. Condition #3 is single IFPM without altitude info. * meets Bonferroni criteria		

Figure 21 and Table 10 show a significant improvement in the TLX ratings for condition 1 as compared to condition 2 and 3. A lower score indicates lower workload. Again, the criteria on the ANOVA tests is that $p<0.05$.

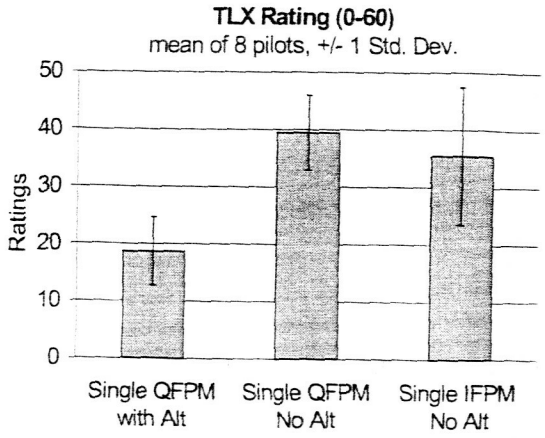

Fig. 21. TLX rating.

Table 10. TLX rating

(3) 1 x 2 ANOVA		
	Mean	**Std. Dev.**
#1	18.73	5.95
#2	39.49	6.52
#3	35.49	11.99
	F Ratio	**p**
1 vs. 2	F(1, 7) = 37.26	Signif., p < 0.01*
1 vs. 3	F(1, 7) = 14.23	Signif., p < 0.03 *
2 vs. 3	F(1, 7) = 2.52	Not significant
Condition #1 is single QFPM with altitude information. Condition #2 is single QFPM without altitude info. Condition #3 is single IFPM without altitude info. * meets Bonferroni criteria		

Figure 22 shows a large and significant pilot preference (lower score) for condition 1 as compared to conditions 2 and 3.

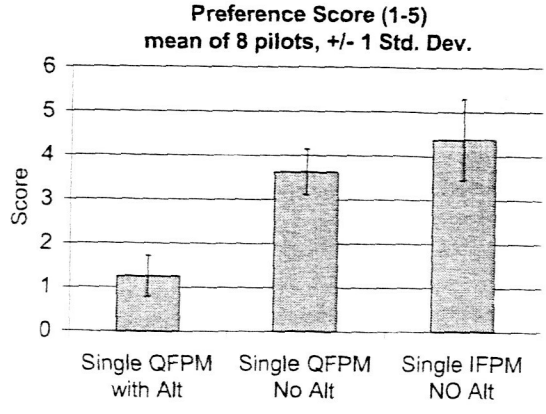

Fig. 22. Preference score.

Table 11. Preference score

(3) 1 x 2 ANOVA		
	Mean	**Std. Dev.**
#1	1.25	0.46
#2	3.63	0.52
#3	4.38	0.92
	F Ratio	**p**
1 vs. 2	F(1, 7) = 168.47	Signif., p < 0.01*
1 vs. 3	F(1, 7) = 112.18	Signif., p < 0.01*
2 vs. 3	F(1, 7) = 3.32	Not significant
Condition #1 is single QFPM with altitude information. Condition #2 is single QFPM without altitude info. Condition #3 is single IFPM without altitude info. * meets Bonferroni criteria		

Discussion of Results

For the particular implementation in this study, adding predictive altitude information, and an altitude target symbol on the display significantly improved pilot altitude control, ground track control, and perceived workload (as measured with the TLX rating). Pilots showed a clear and significant preference for having the predictive altitude information on the QFPM as measured by the preference score.

The other concept evaluated in this experiment is whether multiple QFPMs provide an advantage over a single QFPM. Only evaluated in the horizontal axis, multiple QFPMs showed no advantage to a single QFPM, but added clutter to the display.

Based on the results of this experiment, the recommended symbol is shown in Fig. 23: the single, QFPM with predictive altitude information and an altitude target. This symbol is called an Altitude-Predicting Flight Path Marker (AP-FPM) in this paper. Note that the wings of a traditional FPM were removed for this experiment to de-clutter the multiple QFPM case, but should be included in future designs to be consistent with standard FPMs.

Future Research Areas Identified

Although the AP-FPM worked well, a number of shortcomings were noted. These shortcomings were in the areas of 1) missing graphic information, 2) drive equation issues, and 3) shortcoming in the rendering of the terrain image.

1a) During setup, pilots had difficulty controlling airspeed after a cyclic-pitch input was made. Since the AH-64A symbol set was used as a baseline, only the airspeed digits provided direct airspeed information. This shortcoming of the symbology was bypassed in this experiment by training pilots to keep airspeed constant during the data runs. Constant airspeed was achieved by using collective stick inputs only for altitude control, with no cyclic pitch inputs. For this experiment, constant airspeed was desirable to keep the difficulty of the course the same for all data collection runs. The current synthetic vision simulation at Ames Research Center is investigating the benefit of adding airspeed trend information to the AP-FPM.

1b) Another shortcoming noted during the setup was that there was no indication on the flight path marker as to the maximum climb angle at 100% collective. For this experiment, all hills could be flown over with less than 100% collective at the target airspeed and altitude AGL.

1c) Automatic turn coordination was turned on in this experiment. If automatic turn coordination is not available, then the pilot would have to monitor the sideslip information on the bottom on the screen, visually distant from the AP-FPM symbol.

Figure 24 shows concepts for addressing these three new issues (1a, 1b, and 1c) that were identified in this experiment. The maximum climb angle is depicted as a semi-circle, above the QFPM, drawn at the predicted climb angle at 100% collective. The airspeed control symbol is depicted as a pitch flight director on the right wing, but may also be drawn as a speed error tape and/or longitudinal acceleration caret as is currently implemented on many heads-up displays. The side-slip symbol is depicted as an error tape on the tail.

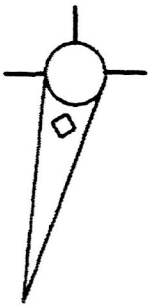

Fig. 23. Recommended Altitude-Predicting Flight Path Marker (AP-FPM).

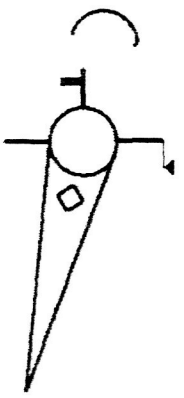

Fig. 24. Future improvement concepts for the AP-FPM.

2a) The first drive equation issue is that the AP-FPM symbol decreases in size at higher speeds (because the 3 second predicted location is farther from the pilot) and increases in size at lower speeds (because the 3 second predicted location is closer to the pilot). This size issue was not a factor in this experiment because airspeed was nearly constant during the data runs. The length of the convergent lines from the QFPM shows the predicted altitude AGL. Therefore, the size of the symbol cannot simply be held constant. The possible solution, currently being tested and not included in this paper, is to make the prediction a fixed distance instead of a fixed time in the future. The distance of prediction may need to be switched to different values for different flight regimes.

2b) The second drive equation issue is what to do when the predicted position is off-screen. This off-screen issue was not a factor in this test because the course and speeds were such that the predicted position was rarely off-screen. However the predicted position is expected to be off-screen in a real operational environment, particularly at low speeds. Therefore, some mechanism should be implemented to limit the movement of the QFPM to the edge of the screen. However, at that point, the predicted altitude information does not conform to the terrain image. An investigation should be done as to whether or not the predicted altitude information should be turned off in this situation.

2c) The third drive equation issue is how to handle steep, ascending, approaching terrain. The terrain in the simulation had terrain with slope within the maximum climb angle of the aircraft at the target airspeed. However, in other geographic locations there may be very steep terrain. A poor design would allow the altitude target diamond on the AP-FPM to suddenly jump in height when the predicted aircraft position encounters the steep slope. Instead, a better design would prematurely drive the target altitude symbol upward to prevent excessive rotor torque.

2d) The fourth drive equation issue is to correct for the target altitude diamond descending prematurely on a new downhill slope, before the aircraft has actually reached the downhill slope. One possible solution, to be investigated, is to have the target altitude symbol show desired altitude above the highest point on the terrain, along the predicted ground track from the current position to the predicted position. In this solution, the display would cause the pilots to error on the high side, instead of the low side when the terrain starts to slope downhill.

3a) The shortcoming in the rendering of the synthetic terrain image was that the photo-textured terrain used (Fig. 25) would interfere with any 2D sensor image of the terrain, such as an infrared camera. A more advanced synthetic vision system would draw the 3D synthetic terrain in a way that does not mask a 2D sensor image of the real terrain. Figure 26 shows one method, in which a wire-frame synthetic terrain overlays the 2D (color) sensor image.

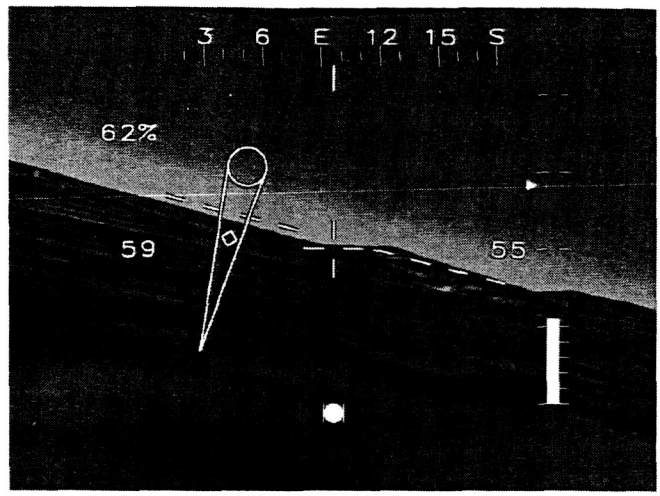

Fig. 25. Photo-textured terrain used in the current experiment.

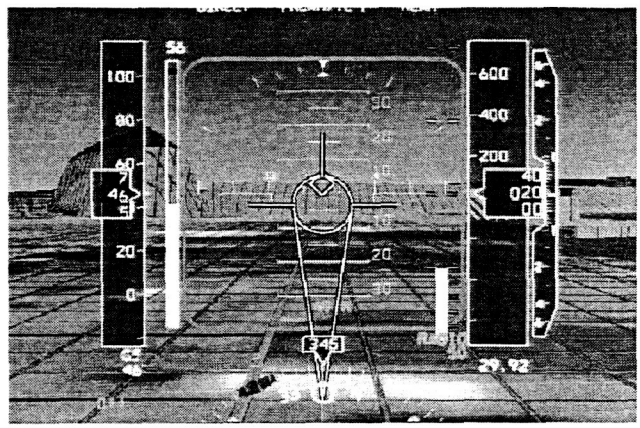

Fig. 26. Wire-frame synthetic terrain over a (simulated) 2D sensor image.

Conclusions

This simulation experiment looked at two potential improvements to the FPM in the context of a panel mounted, synthetic vision display used for flying rotorcraft low level in degraded visual environments.

1) Predictive altitude information was added to the QFPM(s). This concept takes advantage of the fact that a synthetic vision system would know the terrain elevations ahead of the aircraft, from either a sensor or a stored terrain database. Adding predictive altitude information to the QFPM enabled significantly better pilot performance and ratings on all measures taken as compared to that altitude information absent on the QFPM.

2) Multiple copies of the QFPM at different prediction times were displayed as opposed to a single copy at one prediction time. This concept was evaluated only in the horizontal axis in the performance measures. The subjective measures made no axis distinction. All measures showed no statistical difference between the single and multiple QFPM conditions.

Appendix A
Determination of the QFPM prediction point

Variables

a_T	turn angle [deg]
d_{gpn}	horizontal distance north to prediction point [m]
d_{gpe}	horizontal distance east to prediction point [m]
d_{gp}	horiz. resultant distance to prediction point [m]
d_{gph}	vertical distance (altitude) change to prediction point [m], positive up.
f	collective stick input [percent collective]
$F_{hp}( )$	high pass filter [no units]
g	gravitational constant [m/sec^2]
$K_f( )$	gain term for the effect of collective input on the aircraft climb angle [degree climb angle / percent collective]
$K_\theta( )$	gain term for the effect of aircraft pitch on the aircraft climb angle [degree climb angle / degree pitch]
m	mass [kg]
R_T	turn radius [m]
s	Laplace operator
T_p	time of prediction [sec]
T_s	sampling period filter [sec]
u_{ac}	current airspeed [m/sec]
v_{gcr}	current horizontal ground speed [m/sec]
v_{gch}	current vertical speed [m/sec], positive up.
x_{curr}	the value of the filter's current input sample
x_{prev}	the value of the filter's previous input sample
y_{prev}	the value of the filter's previous output sample
θ	pitch [deg]
Φ	roll [deg]
Ψ_{gc}	current ground track, measured -180° to +180°
$\Delta\Psi_{gp}$	horizontal angle between no-turn ground track and ground track with turn [deg]
γ_{gc}	current climb angle, inertially measured [deg]
γ_{gp}	predicted climb angle [deg]
$\Delta\gamma_{gp}$	difference between current and predicted climb angle [deg]
$\Delta\gamma_{gpf}$	difference between current and predicted climb angle due to collective input [deg]
$\Delta\gamma_{gp\theta}$	difference between current and predicted climb angle due to aircraft pitch change [deg]
τ_h	heave time constant of the aircraft [sec]
τ	time constant of the filter [sec]

This appendix provides the mathematical equations for determining the predicted aircraft location. That location is necessary to draw the Quickened Flight Path Marker (QFPM) symbol. Figure A1 defines the notation used. A "Quickened" FPM in the literature refers to a FPM that is an estimation of the future direction of travel of the aircraft, or future position of the aircraft, based on current aircraft state and flight control inputs. The term "quickening" is used in the literature for symbols that have either a prediction in a single axis or in multiple axes. In this paper, "quickening" refers to a prediction of future position in all axes.

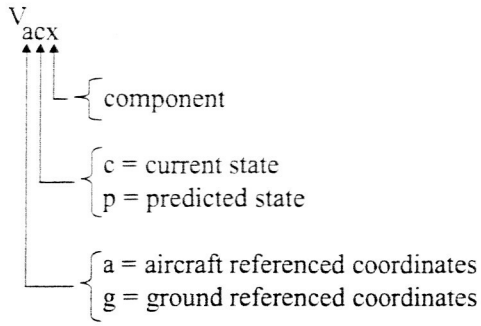

Fig. A1. Definition of subscripts.

There are many ways to estimate future position, with a trade-off existing between complexity and accuracy of the estimation. Experience from this and previous simulations at Ames Research Center have shown that the prediction does not need to be very accurate for pilot performance to improve and pilot workload to decrease. The equations used in this simulation gave a rough prediction of aircraft position, but still enabled substantial improvement in pilot performance by factors of 2-3 in altitude and ground track control. The equations used rely on the measurement of aircraft attitude, ground-referenced linear velocities, and collective stick position.

Figure A2 shows the current and predicted aircraft state in the horizontal plane. The current ground track "Ψ_{gc}" is measured ±180 degrees from north, with positive values measured clockwise. Equations (A1) and (A2) determine the distance the aircraft is expected to travel in north and east direction components for all quadrants.

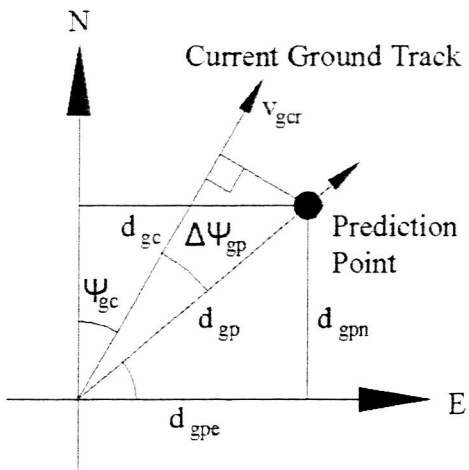

Fig. A2. North-East Quadrant Ground Track.

$$d_{gpn} = d_{gp} \cos(\Psi_{gc} + \Delta\Psi_{gp}) \qquad (A1)$$

$$d_{gpe} = d_{gp} \sin(\Psi_{gc} + \Delta\Psi_{gp}) \qquad (A2)$$

The distance the aircraft is expected to travel along the predicted ground track is approximated by Eq. (A3).

$$d_{gp} \approx v_{gcr} T_p \quad (A3)$$

Equation (A4) determines the difference between the predicted and current ground track angle. This term is the quickening term in the horizontal plane. Equation. (A4) assumes a coordinated turn, in which the lateral acceleration (aircraft coordinates) is zero. The derivation of Eq. (A4) is provided at the end of this appendix.

$$\Delta\Psi_{gp}=(g \tan(\Phi) T_p) / (2 v_{gcr}) \quad (A4)$$

The vertical angles are shown in Fig. A3, where the predicted position vector is rotated around the vertical axis "H" to be in the same plane as the current ground track (as measured along "v_{gcr}"). The expected aircraft altitude change is determined in Eq. (A5).

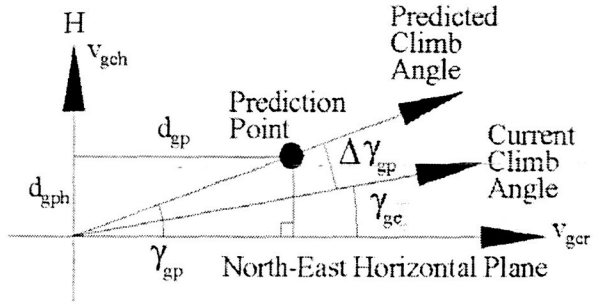

Fig. A3. Vertical profile.

$$d_{gph} = d_{gp} \tan(\gamma_{gc} + \Delta\gamma_{gp}) \quad (A5)$$

The current climb angle is defined in Eq. (A6).

$$\gamma_{gc} = \arctan(v_{gch} / v_{gcr}) \quad (A6)$$

The predicted change in the climb angle, which is the quickening term in the vertical direction, is determined in Eq. (A7).

$$\Delta\gamma_{gp} = \Delta\gamma_{gpf} + \Delta\gamma_{gp\theta} \quad (A7)$$

"$\Delta\gamma_{gpf}$" , determined in Eq. (A8), is an approximation of the change to the steady-state aircraft climb angle, due to collective input. When properly tuned, the parameter "$\Delta\gamma_{gpf}$" decays at the same rate that the angle "γ_{gc}" converges on its steady state value after a collective stick input has been made. The decay time is determined by the time constant "τ" of the high pass filter "F_{hp}".

$$\Delta\gamma_{gpf} = K_f(u_{ac})F_{hp}(f, \tau_h)\cos(\Phi) \quad (A8)$$

The value of the gain "K_f" is a table of the magnitude of changes to the aircraft climb angle vs. changes in collective input, for different airspeeds. "τ_h" is the heave time constant of the aircraft. For better fidelity, "τ_h" may be a table of the heave time constant vs. airspeed, instead of a single value.

"$\Delta\gamma_{gp\theta}$", determined in Eq. (A9), is an approximation of the change in the steady-state aircraft climb angle, due to aircraft pitch changes. When properly tuned, the parameter "$\Delta\gamma_{gp\theta}$" decays at the same rate that the angle "γ_{gc}" converges on its steady state value after a pitch change has been made. The decay time is again controlled by the time constant "τ" of the high pass filter "F_{hp}".

$$\Delta\gamma_{gp\theta} = K_\theta(u_{ac})F_{hp}(\theta, \tau_h)\cos(\Phi) \quad (A9)$$

"K_θ" is a look-up table of the magnitude of changes to the aircraft climb angle changes vs. changes in aircraft pitch, at various airspeeds. "τ_h" is the same heave time-constant, previously discussed.

See Refs. 4, 5, 8 for a more complete discussion of the vertical quickening.

Digital High Pass Filter

An analog high pass filter is modeled with the Bilinear (Tustin) digital approximation. The analog filter is given in Eq. (A10), and the associated digital approximations are given in Eqs. (A11-A13).

$$F_{hp}(s, \tau) = \tau s / (\tau s + 1) \quad (A10)$$

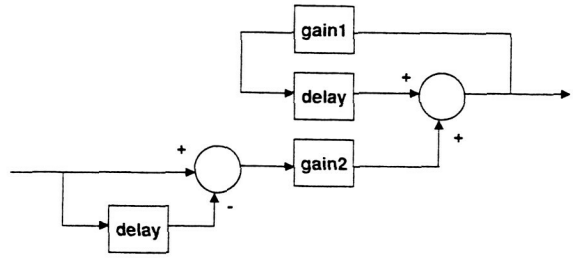

Fig. A4. Digital High Pass Filter.

$$F_{hp}(x, \tau) = \text{gain1}(y_{prev}) + \text{gain2}(x_{curr} - x_{prev}) \quad (A11)$$

$$\text{gain1} = (2\tau - T_s) / (2\tau + T_s) \quad (A12)$$

$$\text{gain2} = 2\tau / (2\tau + T_s) \quad (A13)$$

Derivation of the horizontal angle to the predicted aircraft location

For a steady, coordinated turn (Fig. A5), the aircraft-lateral component of the centrifugal force equals the aircraft-lateral component of the force of gravity, as shown in Eq. (A14).

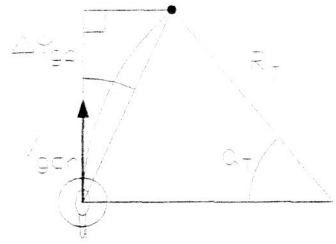

Fig. A5. Horizontal angle to predicted aircraft location.

$$m\,(v_{gcr}^2 / R_T)\cos(\Phi) = m\,g\sin(\Phi) \qquad (A14)$$

$$R_T = v_{gcr}^2 / g\tan(\Phi) \qquad (A15)$$

$$a_T = v_{gcr}\,T_P / R_T \qquad (A16)$$

Equation (A17) is derived by substituting Eq. (A15) into Eq. (A16).

$$a_T = T_P\,g\tan(\Phi) / v_{gcr} \qquad (A17)$$

The angle a_T can be shown to be twice the angle $\Delta\Psi_{gp}$. Making this substitution, the derivation of Eq. (A4) is complete.

$$\Delta\Psi_{gp}=(g\ \tan(\Phi)\,T_p) / (2\,v_{gcr}) \qquad (A4)$$

References

[1]Braithwaite M., Groh, S., Alvarez E., Spatial Disorientation in US Army Helicopter Accidents: An Update of the 1987-1992 Survey to Include 1993-1995, USAARL Report No. 97-13, 1997.

[2]Durnford S., Crowley J., Rosado N., Harper J., DeRoche S., Spatial Disorientation: A Survey of U.S. Army Helicopter Accidents 1987 - 1992, USAARL Report 95-25, 1995.

[3]"Department of Defense Interface Standard For Aircraft Display Symbology," MIL-STD-1787C (draft 2000).

[4]Moralez E., Tucker G., Hindson W., Frost C., Hardy G., "In-Flight Assessment of a Pursuit Guidance Display Format for Manually Flown Precision Instrument Approaches," American Helicopter Society 60th Annual Forum, 2004.

[5]Merrick V., Farris G., Vanags A., "A Head Up Display for Application to V/STOL Aircraft Approach and Landing," NASA TM 102216, 1990.

[6]Hardy G., "Pursuit Display Review and Extension to a Civil Tilt Rotor Flight Director," Guidance, Navigation, and Control Conference, AIAA 2002-4925, 2002.

[7]Franklin J., Stortz M., Borchers P., Moralez E., "Flight Evaluation and Advanced Controls and Displays for Transition and Landing on the NASA V/STOL Systems Research Aircraft," NASA TP-3607, 1996.

[8]Wilkins R., "Use of Predictive Perspective Guidance Displays for Increased Situational Awareness," American Helicopter Society 57th Annual Forum, 2000.

[9]Frost C., Hardy G., "Evaluation of Flying Qualities and Guidance Displays for an Advanced Tilt-Wing STOL Transport Aircraft in Final Approach and Landing," Biennial International Powered Lift Conference, AIAA 2002-6016, 2002.

[10]Hynes C., Franklin J., Hardy G., Martin J., Innis R., "Flight Evaluation of Pursuit Displays for Precision Approach of Powered-Lift Aircraft," *Journal of Guidance, Control, and Dynamics*, AIAA Vol. 12, No. 4, 1989.

[11]Swenson H., Zelenka R., Dearing M., Hardy G., Clark R., Zirkler A., Davis T., Amatrudo G., "Design and flight evaluation of a visually-coupled symbology for integrated navigation and near-terrain flight guidance," Helmet- and Head-Mounted Displays and Symbology Design Requirements, SPIE Vol. 2218, 1994.

[12]Zelenka R., Smith P., Coppenbarger R., Njaka C., Sridhar B., "Results from the NASA Automated Nap-of-the-Earth Program," American Helicopter Society 52nd Annual Forum, 1996.

[13]Coppenbarger R., "A Sensor-Based Automated Obstacle Avoidance System for Nap-of-the-Earth Rotorcraft Missions," Helmet Mounted Displays Conference, SPIE Vol. 2735, 1996.

[14]Rogers S., Asbury C., Szoboszlay Z., "Enhanced flight symbology for wide field-of-view helmet-mounted displays," Helmet- and Head-Mounted Displays VIII: Technologies and Applications, SPIE Vol. 5079, 2003.

[15]Whalley M., "Effects of Longitudinal and Normal Load Factor Envelopes on Combat Helicopter Handling Qualities," NASA TM 4558, 1994.

[16]MIL-STD-1295A, Human Factors Engineering Design Criteria for Helicopter Electro-Optical Display Symbology, 1984 (cancelled).

[17]Hart S., Staveland L., "Development of NASA-TLX (Task Load Index): Results of Empirical and Theoretical Research. In Hancock & Meshakti (Eds.) Human Mental Workload, Amsterdam: North Holland Press, 1988.

[18]Winer B., Brown D., Michels K., Statistical Principles in Experimental Design, 3rd Ed., McGraw-Hill, New York, 1991.